Gutiérrez Cano, JD.; Catalá Civera, JM.; Penaranda-Foix, FL.; Plaza González, PJ. (2022). Improved open-ended coaxial probe for temperature-dependent permittivity measurements of foodstuff at radio frequencies. Journal of Food Engineering. 316:1-8. https://doi.org/10.1016/j.jfoodeng.2021.110823

TITLE OF THE PAPER:

"Improved Open-Ended Coaxial Probe for Temperature-Dependent Permittivity Measurements of Foodstuff at Radio Frequencies."

by

José D. Gutiérrez-Cano [a*], José M. Catalá-Civera [a], Felipe L. Peñaranda-Foix [a], Pedro J. Plaza-González [a]

[a] Instituto ITACA. Universitat Politècnica de València. Camino de Vera s/n.46022 Valencia, Spain.

E-mail: jdgutierrez@itaca.upv.es, jmcatala@dcom.upv.es, fpenaran@dcom.upv.es pedplago@itaca.upv.es

* Corresponding Author. E-mail: jdgutierrez@itaca.upv.es

ABSTRACT

Accurate determination of permittivity is a crucial factor for successfully developing new food processing technologies at radio frequencies. An improved measurement test fixture based on an open-ended coaxial probe was developed to determine the permittivity of lossy food products at radio frequencies as a function of temperature. In order to increase the sensitivity of the permittivity measurements at these frequencies, especially when using a vector network analyzer as a measuring device, the dimensions of the coaxial cell were carefully modeled to consider the range of dielectric losses estimated for food materials. The electromagnetic model was used to retrieve permittivity values from reflection measurements where the entire geometry of the test fixture was considered assuming there was no open radiation or infinite flanges and without the need of reference materials to calibrate the probe. The new cell was validated through permittivity measurements of six saline solutions and then, employed to determine the dielectric properties of cheese sauces and commercial milk samples at 40.68MHz up to 120ºC. The ionic content and temperature had a limited influence on the dielectric constant but highly determined the loss factor.

Keywords: Dielectric properties, Radio frequency, Open-ended coaxial probe, Milk, Cheese sauce

1. INTRODUCTION

Around 30% of the world's total energy consumption comes from the food sector (Food and Agriculture Organization of the United Nations (FAO), 2011). Moreover, a 60% increase in food demand is expected by 2050 due to the growing population (Ladha-Sabur et al., 2019), which will significantly increase the energy demand. Radio frequency (RF) electromagnetic (EM) radiation (3kHz to 300 MHz) has been broadly investigated to replace less efficient traditional heating systems, such as baking and roasting (Awuah et al., 2014), blanching (Zhang et al., 2020), drying (Wang et al., 2020), pasteurization (Li et al., 2017a; Yang et al., 2019), thawing (Erdogdu et al., 2017), cooking (Rincon et al., 2015) or sterilization (Y. Wang et al., 2003).

Unlike traditional heating technologies, where heat transfer is based on radiation, surface convection, or internal conduction (Macana and Baik, 2018), EM heating technologies involve the direct transfer of energy to the food product through the displacements of the elementary particles – electronic, atomic, ionic, and molecular – that constitute the material (Piyasena et al., 2003). In particular, RF heating is mainly affected by dipole rotation and mobility of dissolved ions in the presence of a high-power alternating electric field (Marra et al., 2009; Piyasena et al., 2003), the latter being the primary factor in heat transfer at RF (Jiao et al., 2018).

Permittivity is the most important material property explaining the behavior of food products when exposed to EM energy (Jiao et al., 2018). Hence, it is a key parameter for the design and optimization of RF heating processes. Other critical factors to be considered during EM and thermal analyses of RF heating applications, such as penetration depth, power density, heating rate, or conductivity, are also directly related to permittivity (Piyasena et al., 2003). Permittivity depends on the frequency, temperature, moisture content, chemical composition, density, physical structure, and state of the material (Venkatesh and Raghavan, 2004). The size and shape of the material also influence the selection of an appropriate measurement approach (Krupka, 2006). At microwave frequencies, a wide variety of measurement methods and permittivity data are available for a vast number of materials (Catalá-Civera et al., 2015; García-Baños et al., 2006, 2005; Krupka, 2006), including food products (Datta and Anantheswaran, 2001; Gutiérrez-Cano et al., 2018; Gutiérrez et al., 2017; Meda et al., 2017). However, permittivity data of food products remains scarce on RF heating as compared to microwave frequencies.

In this low frequency range, Sacilik and Colak (2010) designed a coaxial sample holder connected to an impedance analyzer to determine the dielectric properties of corn seeds with different moisture contents at a low-frequency range, from 1 to 100MHz. Yu et al. (2015) used a liquid test fixture from Agilent (16452) and an impedance analyzer to calculate the permittivity values of bulk canola seeds as a function of temperature and moisture content from 5 to 30MHz. Nelson and Bartley (2002), for their part, developed a system based on a small HP-85070B open-ended coaxial probe in combination to a vector network analyzer (VNA) or an impedance analyzer to measure the dielectric properties of food products up to 95ºC at different RF and microwaves frequencies. The materials were inserted into a stainless-steel sample cup mounted in a Delrin water jacket connected to a constant–temperature liquid circulator to set the desired temperature. This system was later used to determine permittivity values of fruit and vegetable tissue samples (Nelson, 2003) or uncooked chicken breast muscles (Zhuang et al., 2007). Wang et al. (2003) built a similar system, also based on the HP-87070B probe, which was part of a stainless-steel pressure-proof test cell surrounded by a temperature-controlled water jacket able to perform measurements up to 130ºC, to encompass the temperatures needed in pasteurization and sterilization processes. The coaxial probe was connected through a high-temperature coaxial cable to an impedance analyzer to cover different RF and microwave frequencies. In this last work, the authors studied the dielectric properties of whey protein mixture/gel, macaroni, and cheese, and, subsequently, other authors used this system with other foodstuffs such as mashed potatoes (Guan et al., 2004), bread (Liu et al., 2009), dried fruit (Alfaifi et al., 2013), or almond kernels (Li et al., 2017b). Analogous systems with open-ended coaxial probes and VNAs were also employed to measure the permittivity values of other food products at RF (Guo et al., 2011; Ling et al., 2015; Zhu et al., 2014; Zhu and Guo, 2017). A common feature in all these studies was the application of the open-ended coaxial probe method; in particular, the high-temperature coaxial probe from Keysight (Keysight Technologies, 2014). However, the small size of this probe could lead to some drawbacks when determining precise permittivity values at RF (Gregory and Clarke, 2007), as well as to noticeable uncertainties when the loss factor was considerably higher than the dielectric constant (Keysight Technologies, 2014), which is to be expected in materials with high ionic content as is the case of food products. Furthermore, these assumption of these models considering an open radiation with infinite flange can cause inaccuracies due to the reflection measurements of metallic walls containing the food material (Muñoz et al., 2018).

In this paper, we describe an improved coaxial test fixture to determine the permittivity of lossy food products at RF as a function of temperature (up to 120ºC). The method is based on an open coaxial cell radiating in a heated pressure-proof stainless-steel cylindrical vessel of appropriate dimensions to improve the accuracy of measurements at these frequencies. Unlike other methods, this vessel was included in the electromagnetic model to increase permittivity precision in order to take into account the longer wavelengths and penetration depth of RF. We assessed the increased sensitivity of this coaxial probe through a detailed uncertainty analysis of the parameters involved in the measurements and validate the measurement method through measurements of saline solutions. Finally, the permittivity values of some commercial foodstuff, such as food sauces and milk, were obtained to demonstrate the convenience of this new set-up.

2. Materials and Methods

2.1. Materials

Cheese dipping sauces and commercial ultra-high temperature-treated (UHT) milk samples were selected as representative of high-loss food materials. All of them were purchased from a local store in Valencia (Spain). The skimmed and whole UHT milk samples were produced by Lidl (Lidl Supermercados, S.A.U., Barcelona, Spain), while the cheese sauces were produced by Mission (Mission Foods Iberia S.A.U., Madrid, Spain) and Santa Maria (Santa Maria AB, Mölndal, Sweden). Table 1 reproduces the nutritional content of the measured food materials as listed in the manufacturers' packaging. The salt content reproduced in the table corresponds to the sodium chloride content of the food product. In addition, the ash content (minerals or inorganic constituents) determined according to AOAC 945.46 is also presented. All materials were stored unopened at room temperature until the time of measurement to avoid material degradation.

In addition, to validate the measurement method, six saline solutions with salinities ranging from 0% to 3.5% weight/volume were prepared by weighing the appropriate amounts of pharmaceutical grade sodium chloride (141659.1210, Panreac Química, Barcelona, Spain) and mixing them with water (361074.1612, Panreac Química, Barcelona, Spain) in a 50ml volumetric flask. The lower sodium chloride concentration corresponded to pure water and the higher to the salinity levels of seawater (Klein and Swift, 1977). A

digital scale with a resolution of 0.01mg (SM1245Di, VWR International, Leuven, Belgium) was used for weighing the sodium chloride quantities.

Table 1. Nutritional contents (Carbohydrates, Protein, Fat and Salt) of the four commercial food samples used in the study as listed in the packaging, in grams per 100g for the cheese sauces and in grams per 100ml for the milk samples. Measured ash content in grams per 100g (Ave±STD over three replicates).

Sample	Carbohydrates	Protein	Fat	Salt	Ash
Mission cheese sauce	6.0	2.2	9.0	1.5	1.79 ± 0.04
Santa Maria cheese sauce	7.4	2.5	9.9	2.0	2.56 ± 0.06
Whole milk	4.6	3.0	3.6	0.13	0.68 ±0.01
Skimmed milk	4.8	3.1	0.3	0.13	0.72 ±0.01

2.2. DIELECTRIC PROPERTIES MEASUREMENT SYSTEM AND EXPERIMENTAL SET-UP

The dielectric measurements were conducted using a custom-built fixture depicted in Figures 1 to 3. The cell consists of an open-ended coaxial probe with a built-in heat sink connected to a cylindrical measurement vessel to locate the material. The dimensions of the open-ended coaxial probe were determined to improve the measurements' accuracy at the ISM frequencies of the RF band. PEI1000 was employed as the filler material (beads) for the coaxial probe (next section). This amorphous and translucent amber thermoplastic material offers excellent heat resistance with a negligible coefficient of linear thermal expansion and consistent dielectric properties over a wide frequency and temperature range.

The sample was placed inside the heating chamber and pushed towards the coaxial aperture by means of a metallic piston that had a recess to collect the excess food material, ensuring that the cylindrical measurement vessel was completely filled with the material to avoid any air gaps. The diameter of the piston was slightly smaller than that of the heating chamber to allow the air to escape from the structure and the sample to rise to the recess to collect the excess material. The chamber was heated by two external heating resistors, regulated by a temperature controller (E5CSV, Omron, Kyoto, Japan) and a type-K

thermocouple. Two O-ring elements, on the top and the bottom of the heating chamber, sealed the pressure inside the heating chamber.

To avoid any damage and calibration drifts of the VNA used to measure the reflection coefficient of the cell, a thermally insulated coaxial section with a built-in heat sink and an air fan coupled to it was employed to reduce the temperature before connecting the coaxial cable to the VNA. As a result, the temperature decreased below 30ºC in the output port of the N transition in both the inner and outer conductors of this coaxial section.

All pieces in contact with the material were made of stainless steel to increase their durability and avoid long-term wear and corrosion. Two polyether ether ketone (PEEK) plates held the heating chamber and provided thermal insulation with the frame of the structure. The heating chamber was finally covered with rock wool to provide additional thermal insulation and protect the user from burns.

2.3. Electromagnetic Model

The electromagnetic response of the measurement device described in section 2.2 was modeled by circuit analysis and mode matching, a well-known technique commonly applied to the analysis of circuits at microwave frequencies (Gutierrez-Cano et al., 2020; Peñaranda-Foix and Catalá-Civera, 2010). The method is based on the segmentation of a complex structure into canonical building blocks that can be analyzed separately as N-port networks, which reduces the complexity of the whole problem (Peñaranda-Foix et al., 2012), and which are then rejoined to characterize the complete geometry.

The analysis of open-coaxial cells is normally addressed by matching the electromagnetic fields at the aperture of a coaxial element radiating towards a dielectric medium, assuming an infinite ground plane and a semi-infinite sample size (Baker-Jarvis et al., 1994; Bakhtiari et al., 1994; Blackham and Pollard, 1997). This approach has also been employed to model coaxial apertures in more complex circuits or resonators using circuit analysis (Canós Marín et al., 2013). However, given that here we have a structure confined by metal walls, we took into account the specific electromagnetic geometry and solved the transition between the coaxial line and the loaded cylindrical waveguide (the cylindrical measurement vessel), assuming there was no radiation nor any infinite flanges. Moreover, by modeling all the elements that make up the geometry of the cell fixture, we could measure at Port 1 performing a classic VNA calibration (open, short, load)

without the need of further calibrations using materials of known permittivity (the typical open, short, water calibration on the aperture of a coaxial probe).

Figure 3 shows the separation of the measurement set-up into canonical elements. From port 1, we established 2 coaxial waveguide sections: the first one is an air-filled coaxial line (Marks and Williams, 1992), which corresponds to the thermally insulated coaxial section, and the second one represents the PEI1000 filled coaxial segment. Next, a circular waveguide filled with a dielectric material, representing the cylindrical measurement vessel, was connected to the second coaxial line. The geometry finishes with a lossy short circuit (Collin, 1990) corresponding to the bottom of the metallic piston.

After computing all the building blocks separately, the reflection coefficient at Port 1, S_{11}, can be retrieved by joining the different networks. From the S_{11} calculation, an optimization process was carried out to determine the dimensions that would maximize the sensitivity of the electromagnetic response of the test fixture in contact with the high-loss materials at RF. Even though coaxial probes can determine permittivity over a broad frequency range, for thermal food processing, only the frequencies selected for industrial, scientific, and medical applications (ISM) in the RF bands 13.56, 27.12, and 40.68 MHz were considered (Jones and Rowley, 1996). The final size of the different parts that make up the probe structure resulted in (see Fig. 3): d_1 = 3mm, d_2 = 6.9mm (N size), and h_1 = 115mm for the coaxial line 1; d_1 = 3mm, d_3 = 12.73mm, and h_2 = 10mm for the coaxial line 2; and h_3 = 40mm and d_4 = 32mm for the cylindrical material housing.

To assess the performance of the above-described measurement set-up, with those dimensions, figure 4 shows the simulation of the reflection coefficient in Port 1 at the ISM frequency of 40.68MHz for a set of dielectric materials ranging from 1 to 200 in the dielectric constant (ε') and from 5 to 2500 in the loss factor (ε''). For a given loss factor, the simulated reflection coefficient as a function of the dielectric constants described an arc whose values are equally spaced in phase. For a fixed dielectric constant, the reflection coefficient formed a straight line with loss factor values, with the spacing decreasing as the loss factor increased. The overall response of the probe diminished as the losses of the materials increased; therefore, a reduced resolution of the dielectric constant is expected for very high-loss materials. As the figure shows, the probe's response offers a wide mapping area providing good sensitivity to discriminate between the permittivity values and the measurement values of the reflection coefficient.

For comparison purposes, figure 4 also depicts the reflection coefficient of an open-ended coaxial aperture with the dimensions of the Keysight 85070B probe, which was calculated for the same set of materials and frequency following the procedure by Baker-Jarvis et al. (1994). As the figure shows, the area of the Smith chart covered by our probe is about 6 times larger, compared to that of the smaller probe for the same set of materials and frequency, what makes it more sensitive to changes in the material's permittivity. The rotation of the mapping is due to the offset added by the coaxial lengths considered in our model. This behavior positively affects measurement uncertainty and demonstrates the suitability of a larger aperture for measurements of lossy food materials at such low frequencies.

From measurements, permittivity was calculated numerically by minimizing Equation (1), which evaluates the absolute difference between the measured (S_{11m}) and the simulated (S_{11}) reflection coefficients using the Nelder-Mead simplex method proposed by Lagarias et al. (1998), available in the *fminsearch* function of Matlab (The MathWorks Inc., Natick, USA).

$$\left| \frac{S_{11}(f, \varepsilon_r, \mu_r) - S_{11m}(f, \varepsilon_r, \mu_r)}{S_{11m}(f, \varepsilon_r, \mu_r)} \right| \quad (1)$$

where ε_r'= complex permittivity (dimensionless), μ_r= complex permeability (dimensionless), and f = resonant frequency (s^{-1}). For food materials, the relative permeability is generally equal to that of free space, μ_r=1 (Datta and Anantheswaran, 2001).

2.4. Uncertainty Study

The total uncertainty of the calculated permittivity was assessed through numerical methods determining the combined standard uncertainty for uncorrelated input quantities as presented in Joint Committee for Guides in Metrology (2008), whose equation is reproduced below:

$$u_c(\varepsilon) = \sqrt{\sum_i \left(\frac{\partial S_{11}}{\partial x_i} \right)^2 \cdot u^2(x_i)} \quad (2)$$

where S_{11} is the simulated reflection coefficient, x_i are the magnitudes involved in that equation showing a noticeable uncertainty contribution, and $u(x_i)$ is the standard uncertainty of those magnitudes. The sources of uncertainty analyzed were the following: dimensional errors due to manufacturing tolerances (±10µm

for d_1 and d_3; ±20µm for d_4; and ±10µm for h_3); errors in the permittivity value of the coaxial bead (±0.05 for ε'); and errors in the measured reflection coefficient, evaluated by estimating the Type A standard uncertainty (Joint Committee for Guides in Metrology, 2008) using 5 independent repeated observations of the reflection coefficient for materials with different losses to cover the mapping of the probe (±0.2º to 5º in phase and ±0.005 in magnitude). The uncertainties due to the length of the coaxial lines (h_1 and h_2) were disregarded since these magnitudes only induce a phase shift that can be easily countered by matching the length of the coaxial lines with the phase of the empty cell.

Figure 5 shows the uncertainty evaluation of the proposed test fixture for the same set of dielectric materials examined in section 2.3. The uncertainty results were superimposed on the corresponding mapping of the reflection coefficient simulated from this set of materials. The cell described here displayed an uncertainty below 5% for the measurement area comprising dielectric constant values above 20 in almost the entire simulated range. Uncertainty increased slightly as the losses increased due to the narrowing of the permittivity map. Uncertainty in the loss factor shows the opposite trend, with uncertainties decreasing as the loss factor values increased, showing a loss factor uncertainty below 5% for the loss factor values above 100 and an uncertainty below 2% for the loss factor values above 250.

The uncertainty analysis allowed us to conclude that the main source of uncertainty derives from the reflection coefficient measurement: we found that phase uncertainty has a significant impact on the uncertainty of the dielectric constant, while magnitude uncertainty basically affects the uncertainty of the loss factor. The magnitude uncertainty also showed a noticeable influence on the dielectric constant uncertainty in the mapping areas close to the center of the Smith chart.

For comparison purposes, Figure 5 also shows the uncertainty obtained for the smaller coaxial aperture using the same sample container and the same sources of uncertainty considered above. This smaller cell exhibited considerably higher uncertainty values than the proposed cell, above 10% in the entire simulated range, being higher than 20% for all values with a dielectric constant below 100. As expected, the uncertainty in the loss factor was also higher, with an uncertainty of about 10% for the loss factor values above 250. It should be noted that using reference materials within the calibration and calculation algorithms could reduce these uncertainties in both cell sizes, but in any case, measurement uncertainties should be taken into consideration.

2.5. Measurement Procedure

The proposed measurement technique was employed to determine the dielectric properties of the food materials described in section 2.1 at the ISM frequency of 40.68MHz. The structure's reflection coefficient was measured by means of a VNA (ZVA50, 2 ports 50GHz, Rohde & Schwarz USA, Inc., Columbia, MD). One hour was allowed to stabilize the VNA prior to calibrating within a range from 10 to 50MHz using a standard OSM calibration procedure with a Type-N calibration kit (53K36R-MSON3, Calibration kit N, 50Ω, Rosenberger, Tittmoning, Germany). The modelling of the reflection coefficient at Port 1, S_{11} in Figure 3, allowed this kind of calibration, avoiding the typical open, short, water calibration of coaxial probes. The cable connecting the VNA and the measurement system remained undisturbed during measurements to avoid calibration drifts (Blackham and Pollard, 1997).

A sample of 35ml of food was put inside the device to fill the measurement vessel and nearly all the housing for excess material, what avoided disturbances from air gaps. The metal piston was tightened with 4 screws applying a torque of 5Nm to avoid leakage and to maintain the pressure of the material inside the chamber during heating. The setpoint of the temperature controller was raised from room temperature (23ºC) up to 120ºC in steps of 20ºC. The thermal stabilization of the material under test was achieved by waiting at least 30 minutes between measurements and verifying that the reading of the reflection coefficient had stabilized. After each set of measurements, the coaxial aperture and the sample vessel were cleaned with deionized water and dried with disposable paper towels. For each plotted point, three heating experiments were carried out with a different sample material, having a total of three replicates at each selected temperature.

3. Experimental Results and Discussion

3.1. Saline Solutions

Figure 6 shows the average dielectric constant and loss factor results at room temperature of the six saline solutions as a function of their salt content. Results in the figure represent the mean value of the three replicates, while the error bars correspond to the uncertainty analysis described in section 2.4.

For comparison purposes, Figure 6 also displays reference values calculated from the Debye equation reproduced below, which contains an additional term ($\sigma/\omega\varepsilon_0$) to include the contribution of ionic conductivity in the dielectric losses (Klein and Swift, 1977):

$$\varepsilon = \varepsilon_{\infty} + \frac{\varepsilon_s - \varepsilon_{\infty}}{1 + \left(j\omega\tau\right)^{1-\alpha}} - j\frac{\sigma}{\omega\varepsilon_0} \qquad (3)$$

where ω is the angular frequency, τ is the relaxation time, α is a parameter to describe the distribution of relaxation times, ε_0 is the permittivity of free space, ε_s and ε_∞ are the lower and upper limits of the dielectric constant respectively, and σ is the ionic conductivity. For saline water, the dependence of these parameters on frequency, temperature, and salinity was provided by Klein and Swift (1977). As the dielectric losses of a sodium chloride water solution at 40.68MHz are mainly affected by ionic dissipation, while the influence of dipole polarization is negligible (Barba and D'Amore, 2012), the loss factor could also be determined from conductivity measurements using the ionic term in Equation (3) (Luan et al., 2015). The conductivity of the six saline solutions was measured by means of a PCE-PHD 1 Multifunction Conductivity Meter (PCE Ibérica S.L., Albacete, Spain) and the calculated loss factor values were included in Figure 6. The presented values are the mean of three replicates and the error bars were determined from the accuracy stated in the manual of the instrument.

Both the dielectric constant and loss factor values showed good agreement with the reference data, having uncertainties below 5% in almost all the measurement range, which validates the performance of the measurement technique at RF.

The dielectric constant of the saline solutions decreased slightly as the salt content increased, in agreement with previous measurements of food samples (Guan et al., 2004). Studies on food materials have highlighted the minor influence of the salt content on the dielectric constant at RF, as dissolved ions reduce polarization and consequently the dielectric constant of water (Ling et al., 2015). However, salt content does have a major impact on the loss factor values at RF. At microwave frequencies, the dielectric losses and, thus, dielectric heating are mainly affected by dipole rotation, while at RF, the ionic mobility of dissolved ions plays the key role (Jiao et al., 2018; Piyasena et al., 2003). The dielectric losses obtained for pure water at 40.68MHz were practically zero, but they increased significantly in the presence of dissolved ions. Hence, the measured loss factor increased from 204.5, for a salt content of 0.25%, to 2312.9, for a salt content of 3.5%. This trend was similar in other works with food materials (Guan et al., 2004; Ling et al., 2015), although the published absolute values of permittivity differ considerably from those of the saline mixtures. The influence of salt content on permittivity depends on how it is bound to other components of

298 the foodstuff that change the mobility of the salts (Icier and Baysal, 2004). Therefore, the characterization
299 of the specific mixed final compound is recommended.

300 These results show the importance of dielectric characterization at RF, since slight variations in the salt
301 level and in the mixture with other base components considerably affect the loss factor values and,
302 consequently, the heating capabilities of food materials using electromagnetic energy. It is also interesting
303 to remark the considerable differences among the loss factor values of these saline solutions at microwave
304 frequencies, given that they increase from 9.6 (0%) to 46 (3.5%) at the ISM frequency of 2.45GHz (Klein
305 and Swift, 1977), which demonstrates the infeasibility of using dielectric properties measured at microwave
306 frequencies in studies at RF.

307

308 ### 3.2. CHEESE SAUCES

309 Figure 7 shows the measured average dielectric constant and loss factor values of the two cheese sauces
310 analyzed as a function of temperature. Although the overall composition of the sauces was different, the
311 loss factor was also found to be directly related to the salt content. At room temperature, the dielectric losses
312 of the Mission sauce (1.5g/100g salt and 1.79g/100g ash) and the Santa Maria sauce (2g/100g salt and
313 2.56g/100g ash) were 840.5 and 976.7, respectively. Both curves are nearly parallel as a function of
314 temperature, reaching very high values at 120ºC, 2365.5 and 2639.2, respectively. This trend is similar to
315 the values reported by Wang et al. (2003), who measured a cheese sauce with an ash percentage of 1%
316 (mass basis), half the ash content than in our sauces, but obtaining, at 40MHz, higher loss factor values
317 over the entire temperature range, from 885.6 at 20ºC to 2985.5 at 121.1ºC.

318 Results of the dielectric constant measurements as a function of the temperature were quite similar for both
319 sauces, although the sauce with the highest salt content showed slightly lower values, probably due to the
320 reduction in polarization caused by the large number of ions (Ling et al., 2015).

321

322 ### 3.3. UHT MILK

323 Figure 8 shows the temperature dependence of the average dielectric constant and loss factor of the whole
324 and skimmed UHT milk samples. The dielectric constant of both milk samples was very similar, although
325 it was slightly higher in the sample with the lower fat content. A decreasing trend was observed regarding

temperature, close to the results presented in section 3.2. Nevertheless, due to the lower loss factor values of milk samples, these measurements were in the broadest part of the probe's response and showed reduced uncertainties, which bolstered our confidence in the results obtained.

The loss factor measurements on the skimmed milk provided higher values than the whole milk (225.2 and 205.4 respectively, at room temperature). This was probably influenced by a higher ionic content in the milk (Moreiras et al., 2013), as the ash content of both samples suggests, and has also been reported by other authors (Guo et al., 2010; Zhu et al., 2014). Once again, both milk samples followed an increasing trend regarding the temperature, reaching values of about 600 at 120ºC.

Nunes et al. (2006) reported the permittivity of UHT milk samples at room temperature for frequencies between 1 and 20 GHz. Their dielectric constant results are in good agreement with our measurements, ceiling the dielectric constant of milk samples to the static dielectric constant of pure water, and obtaining lower dielectric constant values as the fat content increased. They also found a Debye equation for the samples with an additional term for ionic conduction losses, which allows the calculation of permittivity values at 40.68MHz. The loss factor values given by this equation provided 220 for skimmed milk and 225.8 for whole milk, very close to the results shown in Figure 8.

Other studies on permittivity examining different milk samples at RF and performing measurements with an 85070B coaxial probe in combination with a VNA have obtained dissimilar results (Guo et al., 2010, Zhu et al., 2014, Muñoz et al., 2018). At 40.68MHz, some of the trends and permittivity values agreed with our results (Guo et al., 2010, Zhu et al., 2014), whereas others differed (Muñoz et al., 2018). The variability in these published results might be due to uncertainty issues related to the use of small-sized coaxial cells, as described in section 2.4, especially if measurements are carried out with a VNA.

4. CONCLUSIONS

An improved open coaxial test fixture for temperature-dependent permittivity measurements of high loss food products at radio frequencies (RF) was developed. In contrast with previous studies, here, the dimensions of the coaxial cell were carefully modeled to increase the sensitivity of the permittivity determination at RF especially when using a VNA as a measuring device.

The electromagnetic model utilized to retrieve permittivity values from the reflection measurements considered the entire geometry of the test fixture, assuming there was no open radiation or infinite flanges, and without having to use reference materials to calibrate the probe.

The uncertainty analysis undertaken demonstrated the greater accuracy of the used cell compared to most other approaches employed in previous works. The uncertainties in the reflection measurements were found to be the most critical factor in the overall uncertainty. The method's accuracy was also validated by measuring different saline solutions covering the measuring range of the probe with excellent results.

The permittivity of commercial cheese sauces and UHT milk samples was obtained as a function of temperature at the ISM frequency of 40.68MHz. The ionic content and temperature were shown to strongly influence permittivity, particularly the loss factor results. The measured results agree well with those reported by some authors for similar materials, while they differ from the trends found by others. The disparity in the permittivity values reported for similar materials in different works using a similar open-coaxial technique highlights the importance of using a suitable cell size customized for the frequency under study. The use of larger coaxial apertures would be an advisable option to obtain accurate dielectric properties measurements of high-loss materials at RF.

5. Acknowledgments

This paper has been financially supported through the grant reference BES-2016-077296 of the call Convocatoria de las ayudas para contratos predoctorales para la formación de doctores de 2016 by Ministerio de Economía y Competitividad (MINECO) and by European Social Funds (ESF) of European Union.

6. References

Alfaifi, B., Wang, S., Tang, J., Rasco, B., Sablani, S., Jiao, Y., 2013. Radio frequency disinfestation treatments for dried fruit: Dielectric properties. LWT - Food Sci. Technol. 50, 746–754. https://doi.org/10.1016/j.lwt.2012.07.012

Awuah, G.B., Koral, T., Guan, D., 2014. Radio-frequency baking and roasting of food products, in: George B. Awuah, Hosahalli S. Ramaswamy, J.T. (Ed.), Radio-Frequency Heating in Food

Processing: Principles and Applications. CRC press, Boca Raton. https://doi.org/10.1201/b17740

Baker-Jarvis, J., Janezic, M.D., Domich, P.D., Geyer, R.G., 1994. Analysis of an Open-Ended Coaxial Probe with Lift-Off for Nondestructive Testing. IEEE Trans. Instrum. Meas. 43, 711–718. https://doi.org/10.1109/19.328897

Bakhtiari, S., Qaddoumi, N., Ganchev, S.I., Zoughi, R., 1994. Microwave Noncontact Examination of Disbond and Thickness Variation in Stratified Composite Media. IEEE Trans. Microw. Theory Tech. 42, 389–395. https://doi.org/10.1109/22.277431

Barba, A.A., D'Amore, M., 2012. Relevance of Dielectric Properties in Microwave Assisted Processes, in: Costanzo, S. (Ed.), Microwave Materials Characterization. IntechOpen, pp. 91–118. https://doi.org/10.5772/51098

Blackham, D. V., Pollard, R.D., 1997. An improved technique for permittivity measurements using a coaxial probe. IEEE Trans. Instrum. Meas. 46, 1093–1099. https://doi.org/10.1109/19.676718

Canós Marín, A.J., García-Baños, B., Catalá-Civera, J.M., Peñaranda-Foix, F.L., Gutiérrez-Cano, J.D., 2013. Improvement in the accuracy of dielectric measurement of open-ended coaxial resonators by an enhanced de-embedding of the coupling network. IEEE Trans. Microw. Theory Tech. 61, 4636–4645. https://doi.org/10.1109/TMTT.2013.2285359

Catalá-Civera, J.M., Canós, A.J., Plaza-González, P., Gutiérrez, J.D., García-Baños, B., Peñaranda-Foix, F.L., 2015. Dynamic Measurement of Dielectric Properties of Materials at High Temperature during Microwave Heating in a Dual Mode Cylindrical Cavity. IEEE Trans. Microw. Theory Tech. 63, 2905–2914. https://doi.org/10.1109/TMTT.2015.2453263

Collin, R.E., 1990. Field theory of guided waves, 2nd Editio. ed. John Wiley & Sons, New York.

Datta, A.K., Anantheswaran, R.C. (Eds.), 2001. Handbook of Microwave Technology for food applications. Marcel Dekker, Inc., New York.

Erdogdu, F., Altin, O., Marra, F., Bedane, T.F., 2017. A computational study to design process conditions in industrial radio-frequency tempering/thawing process. J. Food Eng. 213, 99–112. https://doi.org/10.1016/j.jfoodeng.2017.05.003

Food and Agriculture Organization of the United Nations (FAO) (Ed.), 2011. Energy-smart food for people and climate. Issue Paper.

García-Baños, B., Catalá-Civera, J.M., Canós, A.J., Peñaranda-Foix, F., 2005. Design rules for the optimization of the sensitivity of open-ended coaxial microwave sensors for monitoring changes in dielectric materials. Meas. Sci. Technol. 16, 1186–1192. https://doi.org/10.1088/0957-0233/16/5/019

García-Baños, B., Cuesta-Soto, F., Griol, A., Catalá-Civera, J.M., Pitarch, J., 2006. Enhancement of sensitivity of microwave planar sensors with EBG structures. IEEE Sens. J. 6, 1518–1522. https://doi.org/10.1109/JSEN.2006.884506

Gregory, A.P., Clarke, R.N., 2007. Dielectric metrology with coaxial sensors. Meas. Sci. Technol. 18, 1372. https://doi.org/10.1088/0957-0233/18/5/026

Guan, D., Cheng, M., Wang, Y., Tang, J., 2004. Dielectric Properties of Mashed Potatoes Relevant to Microwave and Radio-frequency Pasteurization and Sterilization Processes. J. Food Sci. 69, FEP30–FEP37. https://doi.org/10.1111/j.1365-2621.2004.tb17864.x

Guo, W., Wu, X., Zhu, X., Wang, S., 2011. Temperature-dependent dielectric properties of chestnut and chestnut weevil from 10 to 4500 MHz. Biosyst. Eng. 110, 340–347. https://doi.org/10.1016/j.biosystemseng.2011.09.007

Gutiérrez-Cano, J.D., Hamilton, I.E., Catalá-Civera, J.M., Bows, J., Peñaranda-Foix, F.L., 2018. Effect of water content on the dynamic measurement of dielectric properties of food snack pellets during microwave expansion. J. Food Eng. 232, 21–28. https://doi.org/10.1016/j.jfoodeng.2018.03.018

Gutierrez-Cano, J.D., Plaza-Gonzalez, P., Canos, A.J., Garcia-Banos, B., Catala-Civera, J.M., Penaranda-Foix, F.L., 2020. A New Stand-Alone Microwave Instrument for Measuring the Complex Permittivity of Materials at Microwave Frequencies. IEEE Trans. Instrum. Meas. 69, 3595–3605. https://doi.org/10.1109/TIM.2019.2941038

Gutiérrez, J.D., Catalá-Civera, J.M., Bows, J., Peñaranda-Foix, F.L., 2017. Dynamic measurement of dielectric properties of food snack pellets during microwave expansion. J. Food Eng. 202, 1–8. https://doi.org/10.1016/j.jfoodeng.2017.01.021

Icier, F., Baysal, T., 2004. Dielectrical properties of food materials - 1: Factors affecting and industrial uses. Crit. Rev. Food Sci. Nutr. 44, 465–471. https://doi.org/10.1080/10408690490886692

Jiao, Y., Tang, J., Wang, Y., Koral, T.L., 2018. Radio-Frequency Applications for Food Processing and Safety. Annu. Rev. Food Sci. Technol. 9, 105–127. https://doi.org/10.1146/annurev-food-041715-033038

Joint Committee for Guides in Metrology, 2008. Evaluation of measurement data — Guide to the expression of uncertainty in measurement (GUM), JCGM 100:2.

Jones, P.L., Rowley, A.T., 1996. Dielectric drying. Dry. Technol. 14, 1063–1098. https://doi.org/10.1080/07373939608917140

Keysight Technologies, 2014. Keysight 85070E Dielectric Probe Kit 200 MHz to 50 GHz, USA: Keysight Technologies.

Klein, L., Swift, C.T., 1977. An Improved Model for the Dielectric Constant of Sea Water at Microwave Frequencies. IEEE J. Ocean. Eng. 2, 104–111. https://doi.org/10.1109/JOE.1977.1145319

Krupka, J., 2006. Frequency domain complex permittivity measurements at microwave frequencies. Meas. Sci. Technol. 17, R55–R70. https://doi.org/10.1088/0957-0233/17/6/R01

Ladha-Sabur, A., Bakalis, S., Fryer, P.J., Lopez-Quiroga, E., 2019. Mapping energy consumption in food manufacturing. Trends Food Sci. Technol. 86, 270–280. https://doi.org/10.1016/j.tifs.2019.02.034

Lagarias, J.C., Reeds, J.A., Wright, M.H., Wright, P.E., 1998. Convergence properties of the Nelder-Mead simplex method in low dimensions. SIAM J. Optim. 9, 112–147. https://doi.org/10.1137/S1052623496303470

Li, R., Kou, X., Cheng, T., Zheng, A., Wang, S., 2017a. Verification of radio frequency pasteurization process for in-shell almonds. J. Food Eng. 192, 103–110. https://doi.org/10.1016/j.jfoodeng.2016.08.002

Li, R., Zhang, S., Kou, X., Ling, B., Wang, S., 2017b. Dielectric properties of almond kernels associated with radio frequency and microwave pasteurization. Sci. Rep. 7, 42452. https://doi.org/10.1038/srep42452

460 Ling, B., Guo, W., Hou, L., Li, R., Wang, S., 2015. Dielectric Properties of Pistachio Kernels as
461 Influenced by Frequency, Temperature, Moisture and Salt Content. Food Bioprocess Technol. 8,
462 420–430. https://doi.org/10.1007/s11947-014-1413-8

463 Liu, Y., Tang, J., Mao, Z., 2009. Analysis of bread dielectric properties using mixture equations. J. Food
464 Eng. 93, 72–79. https://doi.org/10.1016/j.jfoodeng.2008.12.032

465 Luan, D., Tang, J., Liu, F., Tang, Z., Li, F., Lin, H., Stewart, B., 2015. Dielectric properties of bentonite
466 water pastes used for stable loads in microwave thermal processing systems. J. Food Eng. 161, 40–
467 47. https://doi.org/10.1016/j.jfoodeng.2015.02.014

468 Macana, R.J., Baik, O.D., 2018. Disinfestation of insect pests in stored agricultural materials using
469 microwave and radio frequency heating: A review. Food Rev. Int. 34, 483–510.
470 https://doi.org/10.1080/87559129.2017.1359840

471 Marks, R.B., Williams, D.F., 1992. A general waveguide circuit theory. J. Res. Natl. Inst. Stand. Technol.
472 97, 533–562. https://doi.org/10.6028/jres.097.024

473 Marra, F., Zhang, L., Lyng, J.G., 2009. Radio frequency treatment of foods: Review of recent advances. J.
474 Food Eng. 91, 497–508. https://doi.org/10.1016/j.jfoodeng.2008.10.015

475 Meda, V., Orsat, V., Raghavan, V., 2017. Microwave heating and the dielectric properties of foods, in:
476 Regier, M., Knoerzer, K., Schubert, H. (Eds.), The Microwave Processing of Foods: Second
477 Edition. Elsevier Inc., pp. 23–43. https://doi.org/10.1016/B978-0-08-100528-6.00002-4

478 Muñoz, I., Gou, P., Picouet, P.A., Barlabé, A., Felipe, X., 2018. Dielectric properties of milk during ultra-
479 heat treatment. J. Food Eng. 219, 137–146. https://doi.org/10.1016/j.jfoodeng.2017.09.025

480 Nelson, S.O., 2003. Frequency- and temperature-dependent permittivities of fresh fruits and vegetables
481 from 0.01 To 1.8 GHz. Trans. Am. Soc. Agric. Eng. 46, 567–574.
482 https://doi.org/10.13031/2013.12946

483 Nelson, S.O., Bartley, P.G., 2002. Frequency and temperature dependence of the dielectric properties of
484 food materials. Trans. ASAE 45, 1223–1227. https://doi.org/10.13031/2013.9931

485 Nunes, A.C., Bohigas, X., Tejada, J., 2006. Dielectric study of milk for frequencies between 1 and 20

GHz. J. Food Eng. 76, 250–255. https://doi.org/10.1016/j.jfoodeng.2005.04.049

Peñaranda-Foix, F.L., Catalá-Civera, J.M., 2010. Circuital Analysis of Cylindrical Structures Applied to the Electromagnetic Resolution of Resonant Cavities, in: Vitaliy Zhurbenko (Ed.), Passive Microwave Components and Antennas. IntechOpen. https://doi.org/10.5772/9400

Penaranda-Foix, F.L., Janezic, M.D., Catala-Civera, J.M., Canos, A.J., 2012. Full-wave analysis of dielectric-loaded cylindrical waveguides and cavities using a new four-port ring network. IEEE Trans. Microw. Theory Tech. 60, 2730–2740. https://doi.org/10.1109/TMTT.2012.2206048

Piyasena, P., Dussault, C., Koutchma, T., Ramaswamy, H.S., Awuah, G.B., 2003. Radio Frequency Heating of Foods: Principles, Applications and Related Properties - A Review. Crit. Rev. Food Sci. Nutr. 43, 587–606. https://doi.org/10.1080/10408690390251129

Rincon, A.M., Singh, R.K., Stelzleni, A.M., 2015. Effects of endpoint temperature and thickness on quality of whole muscle non-intact steaks cooked in a Radio Frequency oven. LWT - Food Sci. Technol. 64, 1323–1328. https://doi.org/10.1016/j.lwt.2015.07.017

Sacilik, K., Colak, A., 2010. Determination of dielectric properties of corn seeds from 1 to 100 MHz. Powder Technol. 203, 365–370. https://doi.org/10.1016/j.powtec.2010.05.031

Venkatesh, M.S., Raghavan, G.S.V., 2004. An overview of microwave processing and dielectric properties of agri-food materials. Biosyst. Eng. 88, 1–18. https://doi.org/10.1016/j.biosystemseng.2004.01.007

Wang, Wenjun, Wang, Wenjie, Wang, Y., Yang, R., Tang, J., Zhao, Y., 2020. Hot-air assisted continuous radio frequency heating for improving drying efficiency and retaining quality of inshell hazelnuts (Corylus avellana L. cv. Barcelona). J. Food Eng. 279, 109956. https://doi.org/10.1016/j.jfoodeng.2020.109956

Wang, Y., Wig, T.D., Tang, J., Hallberg, L.M., 2003. Sterilization of foodstuffs using radio frequency heating. J. Food Sci. 68, 539–544. https://doi.org/10.1111/j.1365-2621.2003.tb05708.x

Wang, Yifen, Wig, T.D., Tang, J., Hallberg, L.M., 2003. Dielectric properties of foods relevant to RF and microwave pasteurization and sterilization. J. Food Eng. 57, 257–268. https://doi.org/10.1016/S0260-8774(02)00306-0

513 Yang, Y., Geveke, D.J., Brunkhorst, C.D., Sites, J.E., Geveke, N.J., Tilman, E.D., 2019. Optimization of
514 the radio frequency power, time and cooling water temperature for pasteurization of Salmonella
515 Typhimurium in shell eggs. J. Food Eng. 247, 130–135.
516 https://doi.org/10.1016/j.jfoodeng.2018.12.004

517 Yu, D.U., Shrestha, B.L., Baik, O.D., 2015. Radio frequency dielectric properties of bulk canola seeds
518 under different temperatures, moisture contents, and frequencies for feasibility of radio frequency
519 disinfestation. Int. J. Food Prop. 18, 2746–2763. https://doi.org/10.1080/10942912.2015.1013630

520 Zhang, X., Shi, Q., Gao, T., Zhang, Z., Guo, C., Fu, H., Wang, Y., 2020. Developing radio frequency
521 blanching process of apple slice. J. Food Eng. 273, 109832.
522 https://doi.org/10.1016/j.jfoodeng.2019.109832

523 Zhu, X., Guo, W., Jia, Y., 2014. Temperature-Dependent Dielectric Properties of Raw Cow's and Goat's
524 Milk from 10 to 4,500 MHz Relevant to Radio-frequency and Microwave Pasteurization Process.
525 Food Bioprocess Technol. 7, 1830–1839. https://doi.org/10.1007/s11947-014-1255-4

526 Zhu, Z., Guo, W., 2017. Frequency, moisture content, and temperature dependent dielectric properties of
527 potato starch related to drying with radio-frequency/microwave energy. Sci. Rep. 7, 1–11.
528 https://doi.org/10.1038/s41598-017-09197-y

529 Zhuang, H., Nelson, S.O., Trabelsi, S., Savage, E.M., 2007. Dielectric properties of uncooked chicken
530 breast muscles from ten to one thousand eight hundred megahertz. Poult. Sci. 86, 2433–2440.
531 https://doi.org/10.3382/ps.2006-00434

532

533

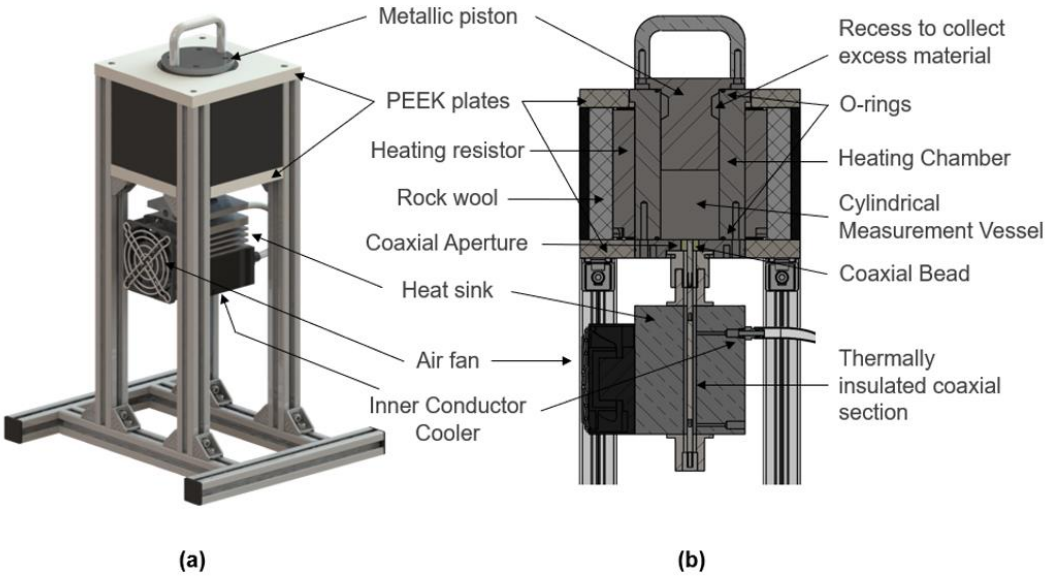

Fig. 1. Schematic view of the open-ended permittivity measurement fixture designed at radio frequencies, (a) rendering image of the external appearance and (b) cut out cross-section of the system.

534

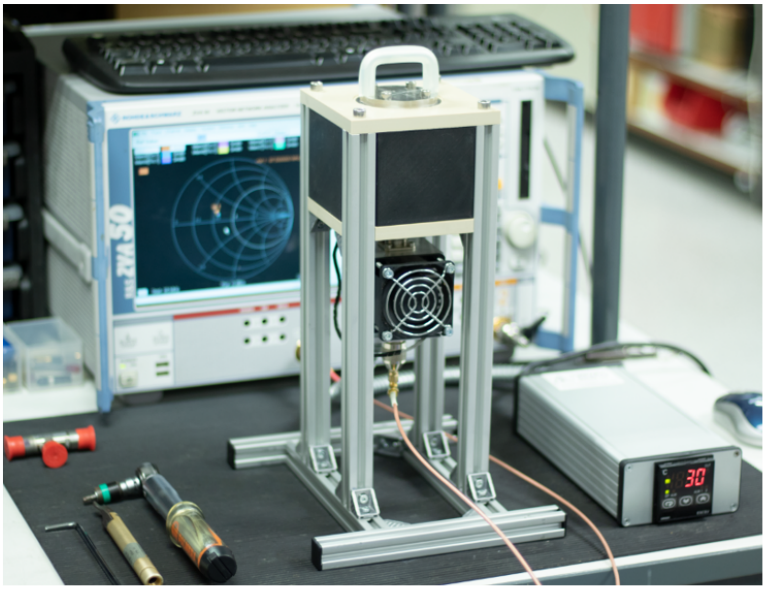

Fig. 2. Picture of the test fixture developed to measure the dielectric properties of food materials at radio frequencies up to 120ºC.

535

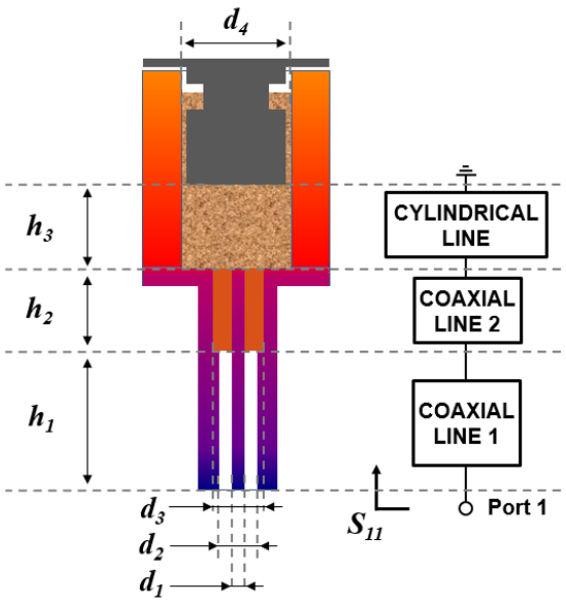

Fig. 3 (a) Geometry diagram of the RF coaxial cell, h_1=115mm, h_2=10mm, h_3=40mm, d_1=3mm, d_2=6.9mm, d_3=12.73mm and d_4=32mm. (b) Circuital representation of the coaxial structure used for mode-matching modelling

536

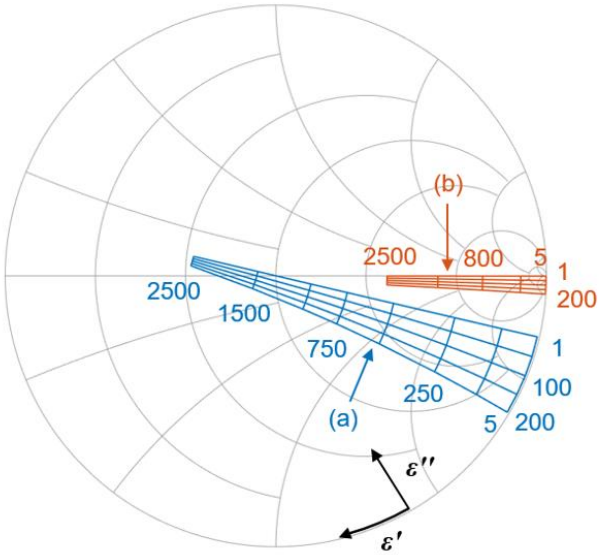

Fig. 4. Mapping of complex permittivity onto the complex reflection coefficient plane (Smith chart) at 40.68MHz for (a) RF coaxial cell with h_1=115mm, h_2=10mm, h_3=40mm, d_1=3mm, d_2=6.9mm, d_3=12.73mm, d_4=32mm and bead permittivity 3 and (b) a coaxial aperture with inner diameter= 0.66mm, outer diameter=3mm and bead permittivity 3.3.

537

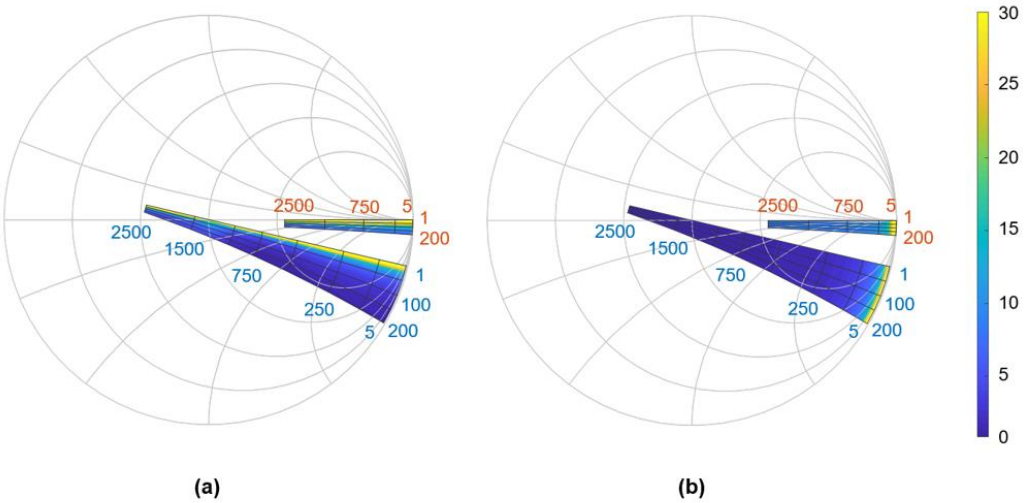

Fig. 5. Uncertainty maps (%) at 40.68MHz for (a) an RF coaxial cell with inner diameter=3mm, outer diameter=12.73mm, bead permittivity 3, h_1=115mm, h_2=10mm, h_3=40mm and d_4=32mm and (b) an RF coaxial cell with inner diameter= 0.66mm, outer diameter=3mm, bead permittivity 3.3, h_1=h_2=0mm, h_3=40mm and d_4=32mm.

538

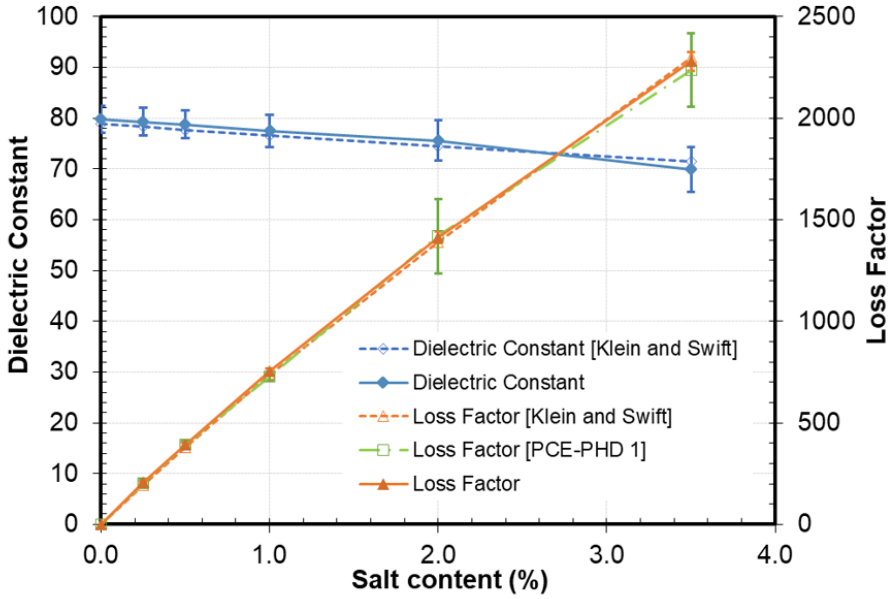

Fig. 6. Dielectric properties at room temperature of different saline solutions as a function of their salt content at 40.68MHz.

539

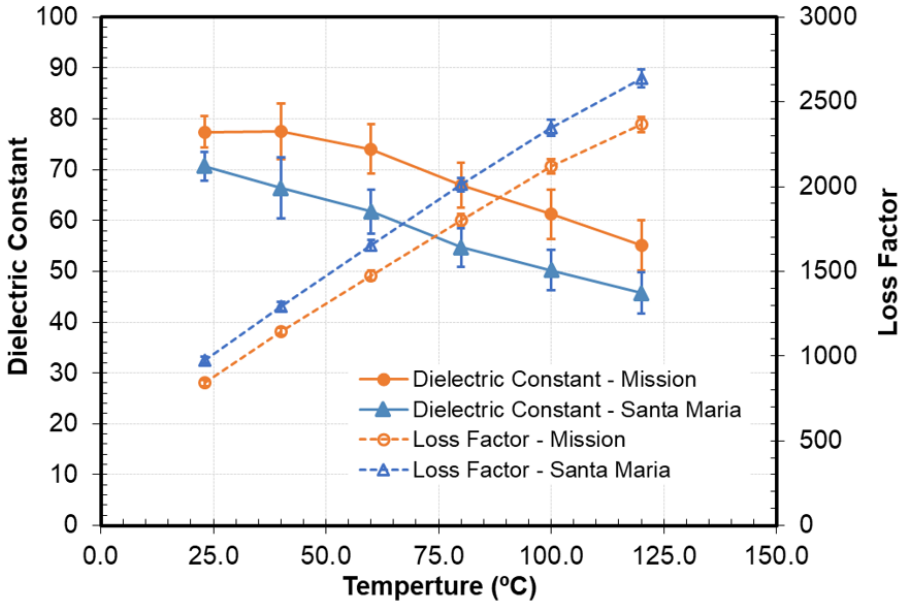

Fig. 7. Dielectric properties of two cheese sauces as a function of temperature at 40.68MHz.

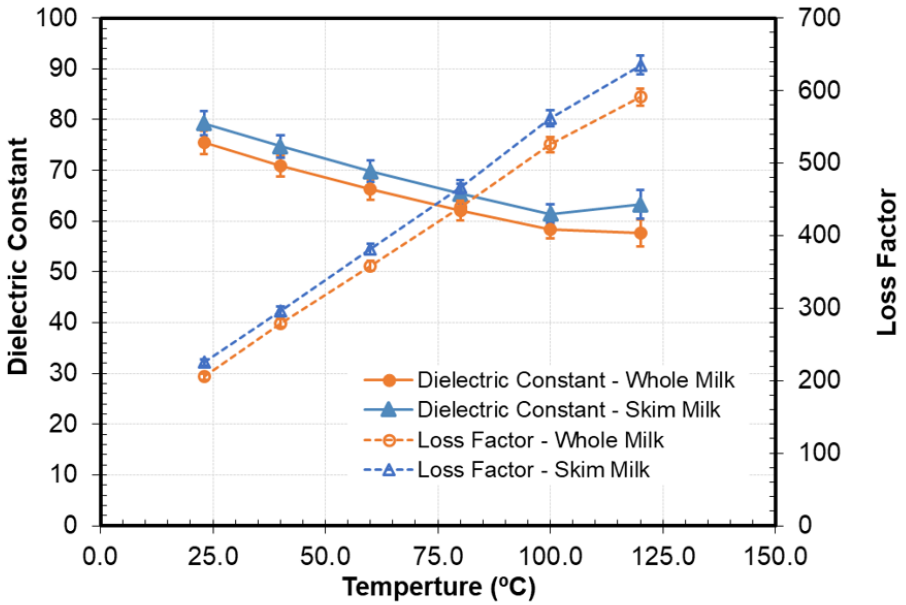

Fig. 8. Dielectric properties of whole and skimmed milk as a function of temperature at 40.68MHz.